Experimental investigation of the hydrodynamic effects upon convecting entropy waves in nozzle flows

S. Mostafa Hosseinalipour[1*], Ebrahim Rahmani[1], Abolfazl Fattahi[2], Nader Karimi[3,4]

[1] School of Mechanical Engineering, Iran University of Science and Technology, Tehran, Iran

[2] Department of Mechanical Engineering, University of Kashan, Kashan, Iran

[3] School of Engineering and Materials Science, Queen Mary University of London, London E1 4NS, United Kingdom

[3] James Watt School of Engineering, University of Glasgow, Glasgow G12 8QQ, United Kingdom

* Corresponding author: asmostef@gmail.com

Abstract

Entropy noise induced by hot spots (entropy waves) is the least explored mechanism of combustion generated sound. Emission of entropy noise is subject to convection of entropy wave throughout the combustor exit nozzle. Nonetheless, the highly diffusive flows in combustors can dissipate entropy waves partially and even totally and hence, suppress the noise generation. Yet, the annihilation of entropy waves in this process is still poorly understood. In particular, no investigation exists on the evolution of entropy waves in nozzle flows. To address this issue, two low-speed, nozzle configurations supplied with fully developed flows at the inlet are examined experimentally. Entropy waves are generated by a controllable electric heater embedded inside the flow. A set of fast-response thermocouples are arranged at the entrance and exit sections of the nozzle to record the spatio-temporal evolution of the entropy wave during its passage thought the nozzle. The acoustic wave, generated by the conversion of entropy waves to sound, is further measured by differential pressure sensors. The results show that hydrodynamic characteristics of the flow such as Reynolds number and turbulence intensity as well as nozzle geometry dominate the survival of entropy wave. Analysis of the spatio-temporal coherence of the wave reveals that there is a predictable frequency threshold above that the wave is spatially distorted. This frequency limit determines the validity range of the commonly used, one-dimensional theoretical models of entropy wave that are currently applied to the whole spectral domain.

Keywords: Entropy wave; Entropy noise; Convective-diffusive waves; Gas turbine combustor; Indirect combustion noise; Spatial coherence.

1. Introduction

Over a century has now passed from the first days of gas turbines. After numerous developments and modifications, gas turbines are currently the key elements of thermal power plants and aero-engines.

Although the modern gas turbines are generally reliable, some defects persist. One of these is the generation of combustion noise with a history longer than that of gas turbines [1]. The unsteady interactions of the flame and flow turbulence cause heat release fluctuations, which then lead to production of the so-called direct noise [2,3]. In addition to this, acceleration of hot spots with distinctive temperature and density, often called entropy wave, results in the generation of indirect or entropy noise [4].

The entropy waves are generated within the flame and travel downstream with the mean flow. They, subsequently, accelerate in the combustor exit nozzle or the first stage of turbine and are converted into sound waves generating noise [4,5,6]. This indirect noise can reflect back into the combustor and intensify the flame unsteadiness and also couple with the combustor acoustics, triggering the low frequency thermoacoustic combustion instability [7-9]. This phenomenon causes a wide range of undesirable effects, from light vibrations and power defect to combustor failure [10]. The fraction of noise entering the surroundings contributes to the environmental noise emission, as one of the main sources of the engine generated sound [11,12]. In recent years, there has been a significant emphasis on the reduction of noise and air pollutant emissions by the civil aviation and power generation sectors [13]. The clean, quiet and stable combustion in both land-based gas turbines and aero-engines has therefore received increasing attention [9,14,15]. This highlights the importance of understanding the mechanisms of noise production in gas turbines. Despite all the research efforts on the noise generation in gas turbines, the indirect (entropy) noise has remained largely unexplored. In the followings, the existing literature on entropy noise is briefly reviewed.

The seminal work of Marble and Candel [5] on the conversion of entropy waves to acoustic perturbations commenced the research activities around indirect noise and, remained as a key reference for more than forty years. Following a few decades of gap, many efforts was made to release the simplifying assumptions of the model of Marble and Candel [5] such as linear wave and compact nozzle [16-21]. Yet, the assumption of one-dimensionality of entropy wave remained as an essential element of these analyses. This was, in part, due to the lack of experimental data on the spatial coherence of entropy waves. The early experimental attempts to detect entropy waves and noise were rather limited in accuracy. For example, Zukoski-Auerbach [22] used an electrical heater with 1K temperature magnitude and recorded a barely detectable resultant acoustics. More recently, Hield et al. [23] showed experimentally that the entropy noise could significantly contribute to the thermoacoustic stability of a premixed combustor with chocked nozzle. In a recent study, Li et al. [24] conducted the portion of the entropic energy in the total energy growth in a triggering unstable system. It was found that entropic energy conversion to acoustics may intensify the total energy by a factor of two. The work of Li et al. [24] also reconfirmed that neglecting entropic modes could severely affect the prediction of combustor stability margins.

Bake et al. invented the "entropy wave generator" (EWG) [25-27] and used the apparatus in a series experimental works. They employed an electrical heater to generate entropy wave and evaluated the resultant acoustic waves emitted by accelerating the entropy waves through a convergent-divergent nozzle. Bake et al. [27] found that the indirect noise is highly depended on the nozzle Mach number [25,26]. Considering the transmitted noise emissions, the experimentally measured data were in fair agreement with the theoretical predictions of Marble and Candel. Importantly, however, Bake et al. made no attempt to study the spatial evolution of the entropy wave. Most recently, Hosseinalipour et al. [28] evaluated experimentally the spatial coherence of the convective entropy waves in a low-speed channel flow. These authors used a network of fast-response thermocouples located at different axial locations along the channel and explored the temporal and spatial decay of the wave [28]. This study was constrained to simple channels, and thus constant mean flow velocities, and did not consider variable cross-sectional areas.

Separating the direct and indirect noise emissions is an important difficulty in interpreting experimental data on indirect noise [29]. Historically, this has led to underestimation of indirect noise, especially in the real-scale combustors [23,30]. The classical two-microphone technique [25-27] and elongating convecting time of the entropy wave [29,32] were employed to separate two types of direct and indirect sound. The recent experimental works of Domenico et al. [29,33,34] were performed in somewhat the same test rig of Bake et al. [24,25]. They stated that despite the weaker amplitude of indirect noise in comparison to the direct one in some nozzle conditions, contribution of each type of noise to the combustor acoustics is difficult to identify when they are merged. Domenico et al. [29,32] used a long convective time of the entropy wave to separate the noises. They also derived an analytical model using the experimental data and embedded a pressure loss coefficient in the entropy to acoustic wave transfer function [34].

The entropy waves, being essentially convected hot pockets, are naturally subject to some levels of annihilation imposed by the convecting flow [35]. The early studies ignored the spatial evolution of the waves by assuming one-dimensional entropy waves, which arose controversial results [23,36,37,38]. Although some limited experimental [35,29] and numerical works [39] confirmed that decay mechanisms could affect the wave, the extent of these effects have not been fully determined. This is an important shortcoming, as the spatial evolution of an entropy wave can potentially influence the acoustical response of the combustion system [9]. The entropy wave is expected to be annihilated by thermal and hydrodynamic processes, as the recent work of Fattahi et al. [39] revealed. Through conduction of a large eddy simulation, Fattahi et al. [39] found that hydrodynamic and thermal boundary conditions of the combustor can have a pronounced effect on the decay of entropy wave. This investigation was performed on a flow between two parallel plates and thus did not consider acceleration of the mean flow that occurs in nozzles. Most recently, Weilenmann et al. [40] experimentally investigated the dynamics of entropy waves using acoustically

forced flames in a duct with uniform cross section. It was shown that entropy waves decayed as the excitation frequency and length of the duct increased. The importance of mixing process in decaying entropy waves, particularly for swirled flames, was highlighted. Weilenmann et al. [41] shown that due to the existence of coherent turbulent structures, entropy waves were found to deteriorate faster than the rate predicted by the analytical models. Similar experiments have been carried out by Wang et al. [42], showing that high amplitude and low- frequency acoustic excitation could produce strong entropy waves. The periodic vortex rollup and inner circulation zone fluctuation were introduced as the main reasons for the generation of entropy waves. The vortex shedding was also identified as the reason for dissipation of entropy waves.

The entropy wave can travel through conduits with non-uniform cross sections (e.g. nozzles). This is especially the case when entropy waves reach the first stage of turbine blades that are essentially nozzle-like passages. The existing studies indicate that the state of flow has a pronounced effect upon the entropy wave [19,20,28,39]. Although fluid flow in a nozzle is significantly different to that in a straight duct, so far all studies on the dynamics of entropy waves have been focused on straight channels [9,14, ,36,40,41]. Therefore, there is a clear gap in the literature about the evolution of entropy waves as they pass through nozzles. To resolve this issue, the present experimental work investigates the spatial decay of an entropy wave during its passage through a converging nozzle. Further, the reflected and transmitted noise, emitted by entropy wave accelerating through the nozzle, are detected.

2.Experimental methods

2.1. The test rig

The core of the experimental setup consists of a long smooth pipe with a converging nozzle installed at its exit point. The length and the inner diameter of the pipe are 400mm and 113mm, respectively. Two different nozzle shapes, with the convergent angle of 5 and 18 degree and the length of 200mm, (see Fig. 1), were manufactured and installed at the exit point of the pipe (see Fig. 4). NZ1 and NZ2 denote nozzles (a) and (b) shown in Fig. 1.

The airflow was supplied by a centrifugal compressor and measured by a rotameter. The flow was calmed in the settling chamber and then was made uniform by passing through the flow straightener. The turbulence intensity was controlled by inserting several metal mesh in the flow. To make the longitudinal velocity constant, the flow was passed through hydrodynamic entrance length to reach the fully developed conditions. This was verified by a hotwire anemometer in a set of points on the pipe cross-section. The turbulence intensity of the flow was also measured by the hotwire anemometer at the center of the pipe. Fig. 2a provides a schematic view of the experimental setup.

The entropy wave was generated by an unsteady electrical heater as discussed later. By using flanges, the heater was placed at the cross-section of the pipe, upstream of the nozzle entrance. The produced hot pockets of air were then convected through the duct by the air inertia and formed the entropy wave. This was then detected with the fast-response thermocouples at the exit cross-section of the nozzle. Further, the resultant transmitted and reflected acoustic wave were measured using pressure sensors, depicted in the next section.

2.2 The pressure measurement

The low-pressure differential pressure sensors with the repeatability of 0.25% were flush mounted on three different locations, which are just after the heater (P1), on the nozzle entrance (P2) and at the nozzle outlet (P3), as Fig. 2b depicts. These sensors translate pressure fluctuations into a voltage via a diaphragm or a cantilever beam exposed to the incident sound pressure, using cavities and vents as pressure equalization channels. Two sensors were located opposite each other to calculate the pressure using the arithmetic average. The long pipe with the length of 1200mm and the inner diameter of 113mm, installed at the nozzle upstream, aided to separate the direct and indirect noise by increasing the convective time of the entropy wave (see Refs. [25,26,29,32]). The sensor signals were amplified using a Flyde FE-379-TA amplifier and acquired and sampled using a homemade data acquisition board with frequency of 10 KHz and resolution of 16-bit. The raw pressure signal was phase-averaged for 25 heater pulses, and then filtered to eliminate oscillations at the power frequency signal. The hydrodynamic noises were also filtered using the data obtained under cold flow condition.

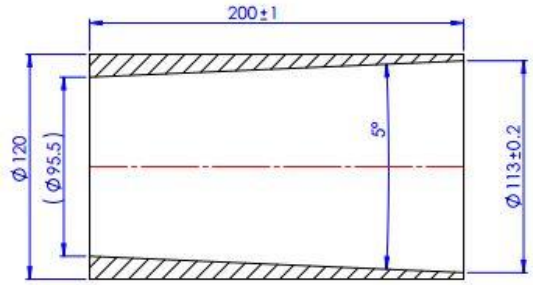

(a)

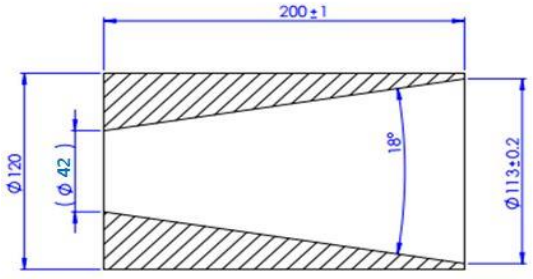

(b)

Fig. 1. Two different nozzle configurations used in the experiments with the convergent angle of (a) 5°and (b) 18°.

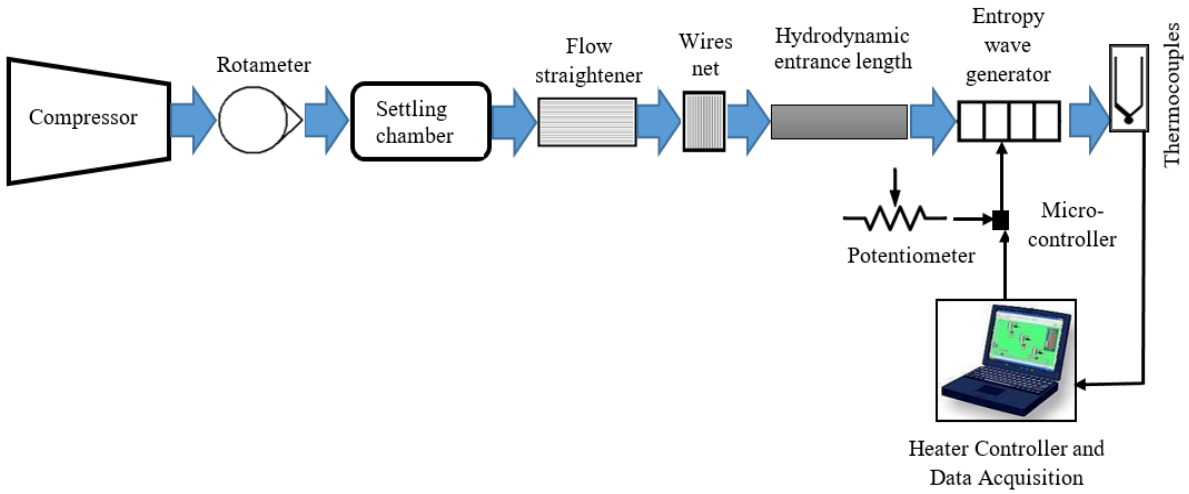

(a)

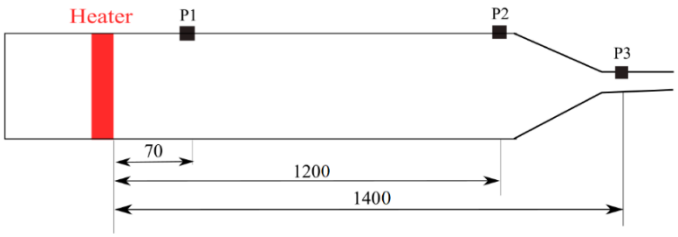

(b)

Fig. 2. The schematic view of (a) the test rig and (b) locations of the pressure sensors (the lengths are in millimeter).

2.3 Entropy wave generation

It is inferred from the thermodynamic relations that in a flow with no acoustic waves, the entropy wave reduces to a temperature fluctuation ($\frac{s'}{c_p} = \frac{T'}{T}$) [26,27]. Therefore, in such flows, temperature perturbations can represent entropy waves. As stated earlier, a controllable electrical heater was used in this study to generate entropy waves. This is similar to the method of entropy wave generation in the works of Bake et al. [26]. Fig. 3 shows the electrical heater used to generate entropy waves in the current study. Further, details about the specifications and manufacturing of the heater can be found in Ref [28].

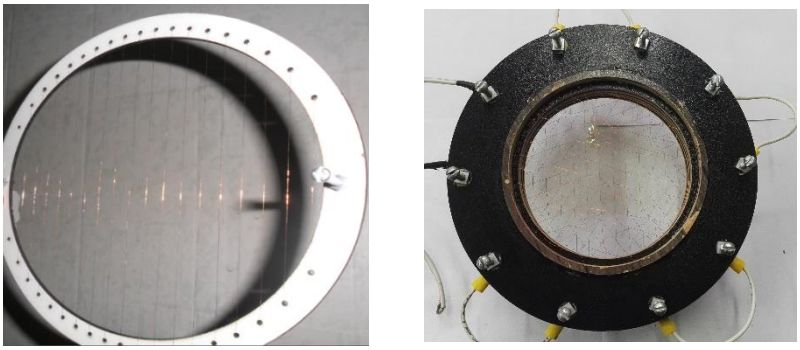

(a) (b)

Fig. 3. (a) A single ring with the wire stretched across, (b) the heater module manufactured using five single rings.

2.4. Fast-response thermocouples

Given the difficulty of measuring a convective thermal wave, fast response probes should be applied to detect the temperature precisely. For the reasons of cost-effectiveness comparing with systems like LIGTS [29] and keeping with the previous measurement techniques [17,23,30], K-type thermocouple probes were manufactured and employed in the current experimental setup. The time constant of the thermocouple response, τ, which equals $\frac{\rho D c_p}{4h}$ [17], can be calculated using the lumped approach under assumptions of first order linear system for the thermocouple wire as a simple cylinder. Considering maximum frequency that can be detected in the electrical devices due to technical limitation, the thermocouple wire diameter of 80μm, indicating maximum frequency of 42Hz, was applied. The thermocouple wires were joined together without using any external material by TIG (Tungsten Inert Gas) welding technique.

The thermocouple probes were set in the experimental setup to measure the temperature rising. This holds the calibration procedure non-mandatory. Nonetheless, the calibration was performed by comparing the data of the current and miniature thermocouple made by OMEGA under steady and transient thermal conditions.

The wave was detected using five-joint thermocouple distribution, in which the probes were arranged on two different radii (0.1 and 0.4 of the inner radius) with a 90° angle shift with respect to each other. This arrangement, demonstrated in Fig.4a, was used on just downstream of the heater and last surface of the nozzle. Fig.4b shows the whole parts of the long current experimental setup, which was schematically depicted earlier in Fig. 1. The last part of the experimental setup is the convergent nozzle, attached at the end.

Figure 4b shows the voltage amplifier and the recording data system installed on a board. This involves five ICs with model of AD595AQ and two boards of Arduino MEGA2560, equipped with 16 analogue channels and a 10bit microprocessor with the sampling frequency of 10 kHz.

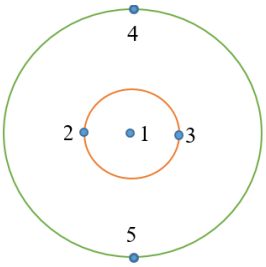

(a)

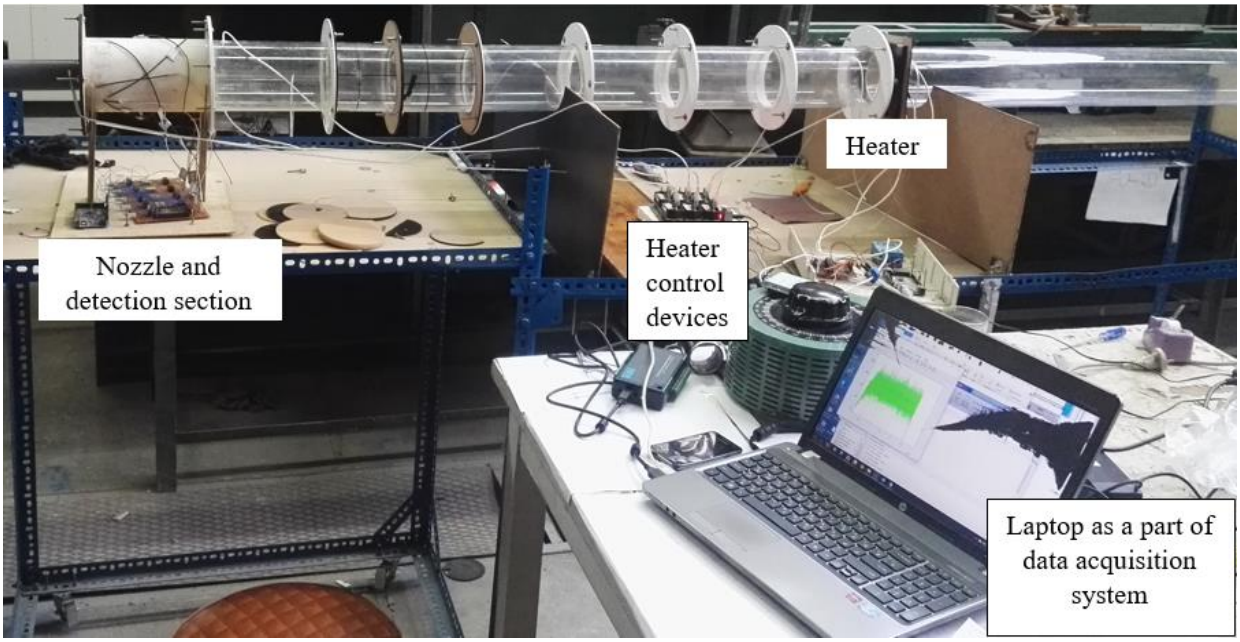

(b)

Fig. 4. (a) Arrangement of the thermocouples in the detection section. Orange and green lines show respectively the inner and outer radius (or orbit), (b) the overall view of the test setup with the detection section installed on the nozzle.

2.5. Test cases

Previous studies confirmed the effects of flow hydrodynamics on entropy waves [33,34,39]. Hence, turbulence intensity and Reynolds number [39] were varied in the current experiments as depicted in Table 1. However, the wave amplitude and width were set constant at the maximum (288W of heater power) and

minimum (0.15s for the duration of heater running) values that the experimental setup could hold. The reasons for the selection of the Reynolds numbers listed in Table 1 have already been in discussed in Ref. [39]. In short, this is to provide an experimental dataset that is comparable to the outcomes of the previous numerical studies. The experiments were performed in the laboratory situated 1200m above the sea level. The temperature of the laboratory varied between 18-23°C, during the experiments.

Table 1- The investigated test cases.

Case No.	Reynolds number	Turbulence intensity (%)
1	13600	2
2	13600	2.8
3	8500	1.1
4	8500	1.4

2.6. Uncertainty analysis

Bias and random uncertainty are commonly found in experimental investigations. The measurement equipment cause bias error, while random error is due to the randomness in the tests [43]. These sources of uncertainty are calculated for the temperature and pressure sensors, separately.

2.6.1. Thermocouples

The resolution of the data acquisition, parasitic voltage and uncertainty in calibration equipment are the origins of the bias error in the current experiments. Considering the measured values for the resolution of the Arduino microcontroller ($b_1 = 0.025$℃), voltage disturbance due to connectors and solders ($b_2 = 0.185$℃), and uncertainty of calibration thermocouples ($b_3 = 0.123$℃), the thermocouple systematic error, expressed by

$$b = \sqrt{b_1^2 + b_2^2 + b_3^2}, \tag{1}$$

is 0.22℃. Assuming the weight factor of $t = 2$ [44], the applied systematic uncertainty will be ± 0.44℃ (95%).

The random error was calculated for all the cases and it was found that case 4 contains the highest random error, discussed here. Having five repetitions ($N = 5$) and five thermocouples ($M = 5$) on the data gathering section, the uncertainty due to non-uniform temperature distribution is calculated by [44]

$$(s_{\overline{\Delta T}_m})_s = \sqrt{\frac{\sum_{m=1}^{M}(\overline{\Delta T}_m - \langle\overline{\Delta T}_m\rangle)^2}{M(M-1)}}. \tag{2}$$

In Eq. (2), $\overline{\Delta T}_m$ and $\langle\overline{\Delta T}_m\rangle$ are respectively the arithmetic average related to the repetition and probe number. Further, uncertainty due to time variations in probe output is given by

$$(s_{\overline{\Delta T}_m})_t = \sqrt{\frac{\sum_{m=1}^{M}\sum_{n=1}^{N}(\overline{\Delta T}_m - \langle\overline{\Delta T}_m\rangle)^2}{MN(M(N-1))}}. \quad (3)$$

Therefore, the total random error is given by

$$s_{\overline{\Delta T}_m} = \sqrt{(s_{\overline{\Delta T}_m})_s^2 + (s_{\overline{\Delta T}_m})_t^2}, \quad (4)$$

which becomes 0.29℃, by considering $(s_{\overline{\Delta T}_m})_s = 0.25$℃ and $(s_{\overline{\Delta T}_m})_t = 0.15$℃.

Finally, the total uncertainty is expressed as

$$u = t \times \sqrt{{s_{\overline{\Delta T}_m}}^2 + b^2}. \quad (5)$$

Using Eq. (5), the net uncertainty for the thermocouples is ± 0.72℃ .

2.6.2. Pressure transducers

According to the manufacturer of the pressure box, the systematic error including repeatability and hysteresis error is $\pm 0.25\%$ of the measured pressure signal. The random error by three repetitions and three replications is achieved 0.64 Pa, using Eqs. (2) to (5).

3. Theoretical Methods

3.1. Coherence analysis

In the course of the experiments, temperature-time series were recorded at each thermocouple junction. The aim is to present the evolution of the wave. In current study, this is done by considering the relation amongst the points on the wave by using the spectral coherence function. This function shows to which extent two sets of data are linearly co-related. Coherence function specifies a value in the range of zero and unity; zero denotes that the two datasets are totally unrelated, while unity indicates a perfect linear relation [45]. For the two signals of x(t) and y(t), spectral coherence is defined as

$$\mathrm{C_{xy}(f)} = \frac{\mathrm{G_{xy}(f)}^2}{\mathrm{G_{xx}(f)G_{yy}(f)}}, \quad (6)$$

where $\mathrm{G_{xx}(f)}$ and $\mathrm{G_{yy}(f)}$ are the auto-spectral density of x and y, respectively, and $\mathrm{G_{xy}(f)}$ is the cross-spectral density. The auto-spectral density functions are computed through applying the mathematical expectation operator, expressed by [45]

$$E[x(t)] = \int_{-\infty}^{+\infty} x(t)p(t)dt, \tag{7}$$

where $p(t)$ is the probability density function. For a discrete variable, the expectation operator equals the sum of multiplication of probability and absolute values of each outcome [38]. The spectral densities are then calculated aiding Fourier transformation, denoted by the capital letters in the following relations.

$$\begin{aligned} G_{xx}(f) &= E[X(\omega)X(\omega)], \\ G_{xy}(f) &= E[X(\omega)Y(\omega)]. \end{aligned} \tag{8}$$

The coherence function was conducted for the convected entropy wave between two cross-sections located at different longitudinal locations. It was also calculated for the temperature-time series captured on two points of the wave front at a given cross-section. The results of coherence function are demonstrated against Strouhal numbers variations, defined as follows.

$$St = \frac{f.D_{eq}}{U_b}, \tag{9}$$

in which f is frequency (Hz), U_b is the bulk flow velocity (m/s) and D_{eq} is the equivalent diameter, calculated as $D_{eq} = \frac{D_i + D_o}{2}$, where D_i and D_o are the nozzle diameter at the inlet and outlet, correspondingly.

3.2. Wave front characterization

During convection of the entropy wave throughout the duct, heat transfer and fluid flow make the wave weaker and wider. The wave's front and rear confront the mixing with the base flow, due to turbulent and molecular diffusion, making them undetectable. In the current study, the wave's rear was identified by using the following criterion,

$$\frac{T_i - T_{base}}{T_{base}} = 0.02, \tag{10}$$

where T_i is the temperature recorded at any thermocouple with the detection cross-section and T_{base} is the temperature of the base flow in the absence of any entropy wave. The wave's front was similarly found by setting the left-hand side of the Eq. (10) to 0.001. In the rest of this paper, the abbreviation of "TC" denotes thermocouple.

4. Results and Discussion

4.1. Temperature-time trace signals of the wave

The entropy wave, as a hot spot, convects through the duct and experiences annihilation induced by turbulent mixing, heat transfer and hydrodynamic non-uniformities in the flow field. The amplitude change and deformation of the wave is investigated in this section. Figs. 5 and 6 show the non-dimensional temperature rise, i.e. $\Delta T/T_{base\ flow}$, versus time for the duration of wave convection through the heater to

the nozzle outlet. Here, ΔT is the temperature rising caused by the wave and $T_{base\ flow}$ is the base flow temperature prior to the addition of the wave. For conciseness reasons and due to similar behavior, the results of NZ2 are not presented here. Time zero corresponds to the beginning of the recording by the data acquisition system. The data are presented for two inner (TC 1-3) and outer (TC 4 and 5) radii, as Fig. 4a shows. Figs. 5a and 6a present the entropy wave, just at the heater downstream (3 cm of the heater downstream, called hereafter the inlet), which is less affected by the flow hydrodynamic, while Figs. 5b and 6b demonstrate the wave at the last nozzle surface. The constant heat flux generated by the heater and larger bulk velocity of the maximum Reynolds number (cases no. 1 and 2) cause lower wave amplitude in comparison with that in the case of minimum Reynolds number (cases no. 3 and 4).

The non-dimensional time presented in this figure is defined as $\mathrm{time}/(\frac{L}{U_b})$, in which L and U_b are the duct length and bulk flow velocity, respectively. In all cases, the temperature near the walls (outer radius, TCs 4 and 5) are higher than that on the central zone (inner radius, TCs 2 and 3), due to lower velocity and flow mixing. Further, the wave deformation, or wave widening, is more noticeable at the central zone (inner radius). Despite the wave deformation, the peak moment remains somewhat the same for most TCs at the nozzle outlet. Turbulence intensity appears to be a potential efficacious parameter on wave evolution, highlighted at lower Reynolds number. This is in keeping with the numerical results reported in Ref. [39]. The results show that the evolution of the wave can be directly influenced by the turbulence intensity of the flow. The pointwise and asymmetrically transversal deformation of the wave at the cross section are originated from the inherent features of randomness of turbulent flow.

Figs. 5 and 6 show that, expectedly, the peak in wave amplitude decreases and the width increases during convection through the duct. Figs. 5a and 6a confirm that the wave can be affected by the flow, even at a short convecting length. The turbulence structures and eddies deformation in the energy cascade are the reasons for the decay of entropy wave through the conduit. Although not presented here, the results show that the deformation can be intensified by increasing the nozzle angle, or flow acceleration. This could be caused by strengthening the turbulent mixing and changing the flow residence time in the nozzle.

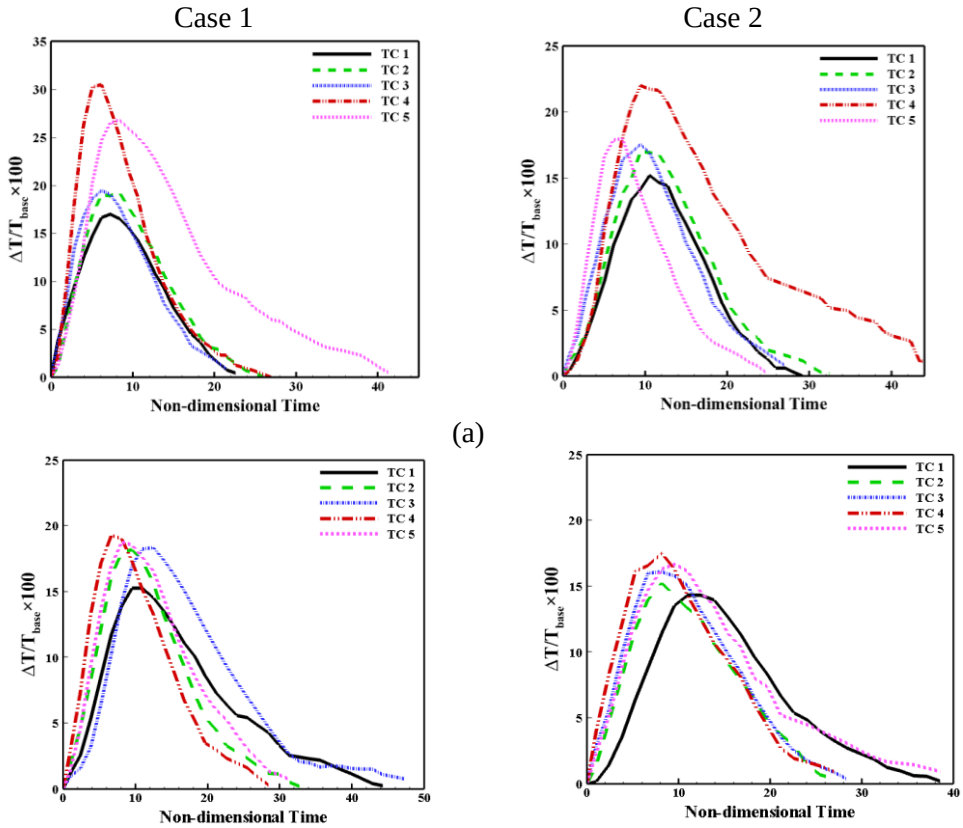

Fig. 5. The time trace of non-dimensional temperature ($\Delta T/T_{base\ flow}$) for cases 1 and 2 at (a) the inlet (heater downstream) and (b) the outlet of the NZ1.

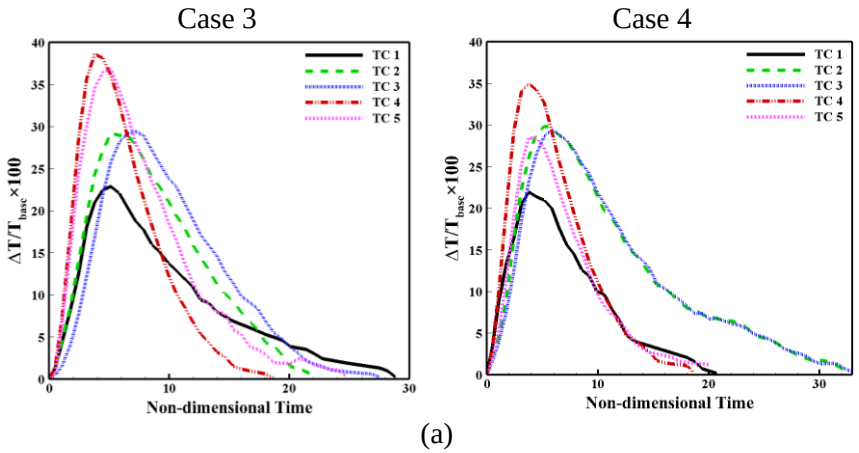

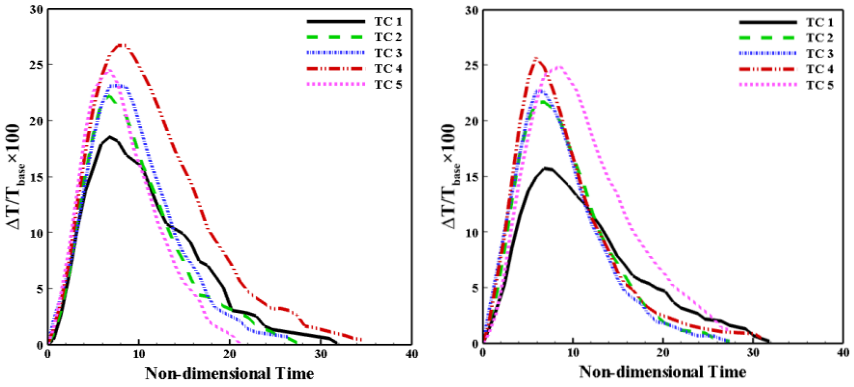

(b)

Fig. 6. The time trace of non-dimensional temperature ($\Delta T/T_{base\ flow}$) for cases 3 and 4; at (a) the inlet (heater downstream) and (b) the outlet of the NZ1.

4.2. The wave coherence

The coherence function for the arithmetic average of temperature signals between the inlet and outlet of the nozzle is depicted in Fig. 7. To present the same range of Strouhal number in all sub-figures, the Strouhal number is chosen twice for the cases of low Reynolds number compared to those of high Reynolds number. For low frequencies, or low Strouhal numbers, the coherence becomes near unity, reflecting the undamaged wave through the convection. This has been also confirmed in the previous works [31-33,39]. Having higher coherence value, the wave remains more coherent at the cases of high Reynolds number or low turbulence intensity. Low coherence values with variations and several peaks and troughs make the wave uncorrelated at low Reynolds number, especially at high turbulence intensity. This is because of the longer residence time of the wave at low Reynolds number, resulting in stronger flow influences upon the wave. Further, increasing the turbulence level intensifies the flow randomness and unsteadiness and adversely affects the wave spatial correlation. This figure implies that the wave evolution becomes less significant as flow acceleration increases. Yet, it is intensified at low Reynolds numbers and high turbulence intensities, reflected by the sever variations and zero coherence values specially found in case 4.

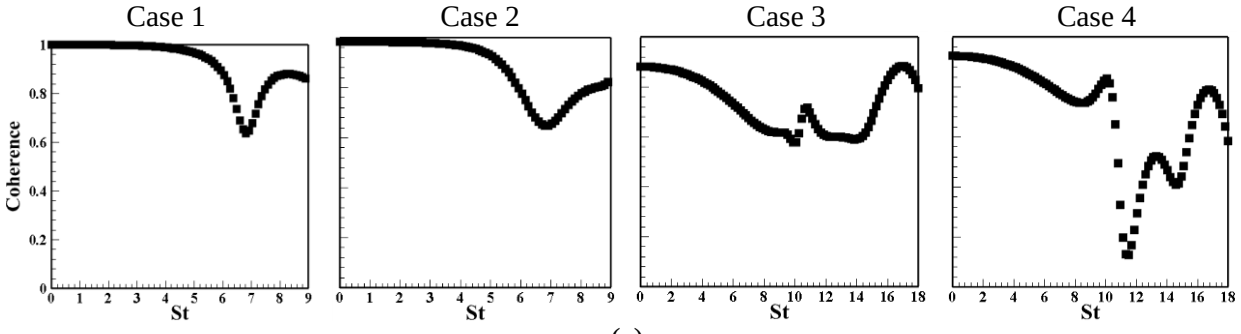

(a)

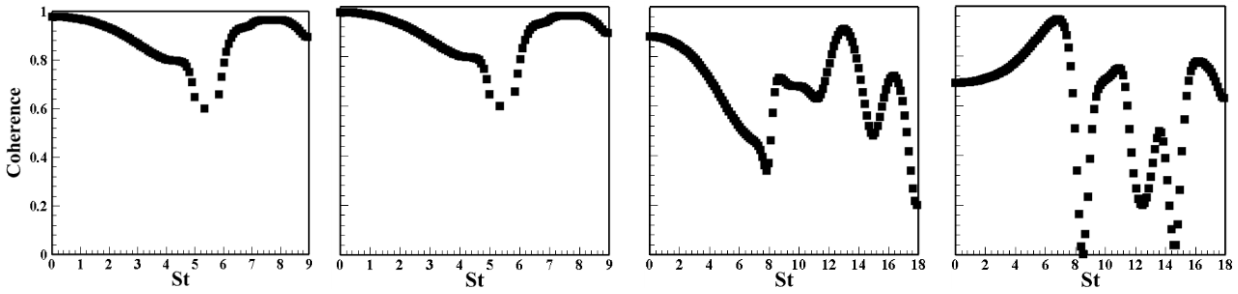

(b)

Fig. 7. Coherence functions for the average temperature signals during convection of the entropy wave between the inlet and the nozzle outlet for (a) NZ1 and (b) NZ2.

Figs. 8 and 9 illustrate the coherence of the wave front for various TCs related to the center. For brevity, only two TCs (TC of 2 and 4) and two cases (no. 1 and 4) are presented here. These figures imply that although the temperature peaks are smaller at the inner radius (see Figs. 5 and 6), the wave remains more preserved in comparison with that at the outer radius. The difference in the wave between two detection radii renders a non-uniform wave due to hydrodynamic effects. As reported previously [41,42], high frequency components, characterized by short time and length scales, can be readily annihilated in all cases by the turbulent flow. Yet, the fully coherent components are found at low Strouhal numbers. Figs. 8 and 9 show a drastic change in the wave amplitude through Strouhal number range by convecting the wave in an unsteady turbulent flow. This represents a frequency-dependent behavior of the wave evolution. The non-uniformity of the wave surface can be explained by noting the anisotropic behavior of the turbulent flow. The heavily location-dependent behavior may diffusively separate the wave to distributed hot spots. Thus, the entropy wave can be hardly described as one-dimensional, except for a narrow frequency range. The peaks and troughs found in the second half of the figure show intensified irregularities, which make the wave's behavior unpredictable at high frequencies. Increasing the flow acceleration results in more damage to the wave coherence.

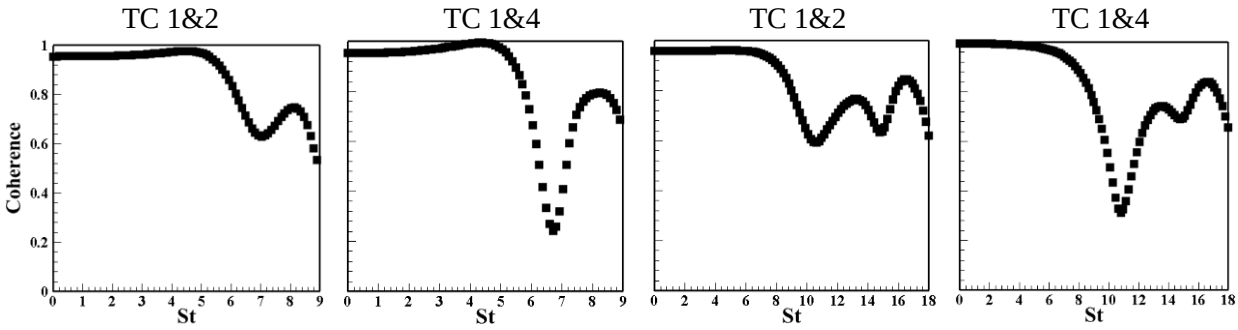

(a) (b)

Fig. 8. Coherence function for the temperature signals between TC 1&2 and TC 1&4 for NZ1; (a) case 1 and (b) case 4.

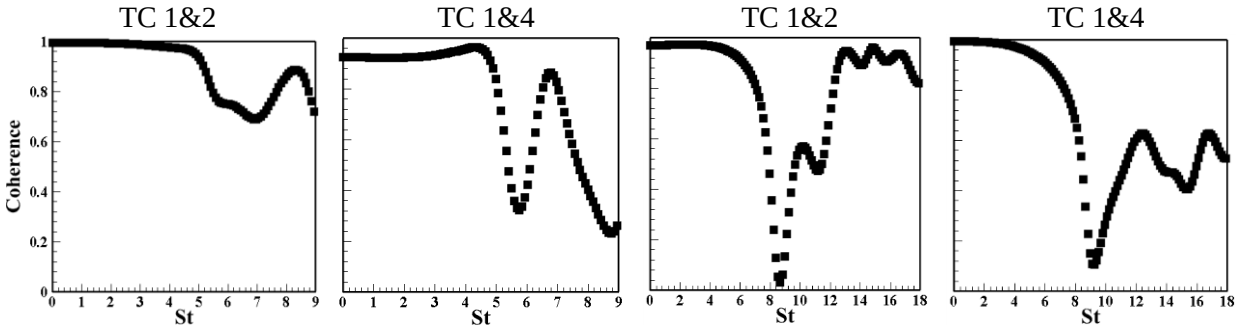

(a) (b)

Fig. 9. Coherence function for the temperature signals between TC 1&2 and TC 1&4 for NZ2; (a) case 1 and (b) case 4.

The current results show that the one-dimensional assumption made in most theoretical and numerical studies of entropy wave can be highly questionable. The average coherence over the cross-section and the standard deviation of the temperature signals are the measures that show whether the wave is uniform on the cross section or not.

The average coherence is defined by an arithmetic average of the coherences calculated from the time traces produced by TC1 (located at the center point) and those located on the cross section, given by the following relation.

$$\overline{\mathrm{Coh}}_{\mathrm{D}} = \frac{\sum_{\mathrm{i}} \mathrm{Coherence}[\mathrm{Thc}_1(\mathrm{t}), \mathrm{Thc}_{\mathrm{i}}(\mathrm{t})]}{\mathrm{n}}, \tag{11}$$

in which, $\mathrm{Thc}_{\mathrm{i}}(\mathrm{t})$ is the time trace obtained from the thermocouple i on the cross section and n is the number of coherence operation between thermocouple 1 and the other thermocouples. Subscript D indicates that the calculation of coherence is carried out over the cross-section of the flow conduit. Standard deviation, as a quantity for data spreading around the mean, is used to infer the wave uniformity in the frequency domain. This is calculated by

$$\mathrm{SD}_{\mathrm{D}}^2 = \frac{[\mathrm{Coherence}(\mathrm{Thc}_1(\mathrm{t}), \mathrm{Thc}_{\mathrm{i}}(\mathrm{t})) - \overline{\mathrm{Coh}}_{\mathrm{D}}]^2}{\mathrm{n}}. \tag{12}$$

SD_{D} indicates how much variation in the wave coherence occurs over the cross-section of the nozzle as the wave convects from the heater to the nozzle outlet. Fig. 10 depicts $\overline{\mathrm{Coh}}_{\mathrm{D}}$ and SD_{D} for the wave at the inlet and outlet of the nozzle. According to this figure, the wave uniformity can be highly influenced shortly after leaving the heater. An exception to this is the case with high Reynolds number and low turbulence intensity. As an important result, Fig. 10 indicates that the assumption of one-dimensional wave may hold at low Strouhal numbers, with wavelength threshold about the same for all cases (corresponds to $\mathrm{St} \cong 4$ for cases 1 and 2 and $\mathrm{St} \cong 8$ for cases 3 and 4). The $\overline{\mathrm{Coh}}_{\mathrm{D}}$ value is greater than 0.5 for the NZ1, demonstrating that despite losing the spatial coherence, the wave is not fully annihilated by the flow and remains somewhat

correlated. This is similar to the findings about the survival of entropy wave through adiabatic duct flow with zero acceleration [36,46]. However, higher flow acceleration in the steeper slope nozzle (NZ2) intensifies the wave non-uniformity and eliminates the chance of wave survival, except at low Strouhal numbers. A more drastic variation could be found in a real combustor, not only due to diffusion and turbulent mixing, but also owing to large heat losses from the combustor walls [39]. Considering the high value of SD_D at high frequencies, the wave becomes annihilated through a non-uniform diffusion as also shown in Fig. 9. Although the values of SD_D for cases 3 and 4 of NZ1 and cases 1 and 2 of NZ2 largely grow with frequency increment, the average coherence is mostly above 0.5, noting a semi-correlated wave.

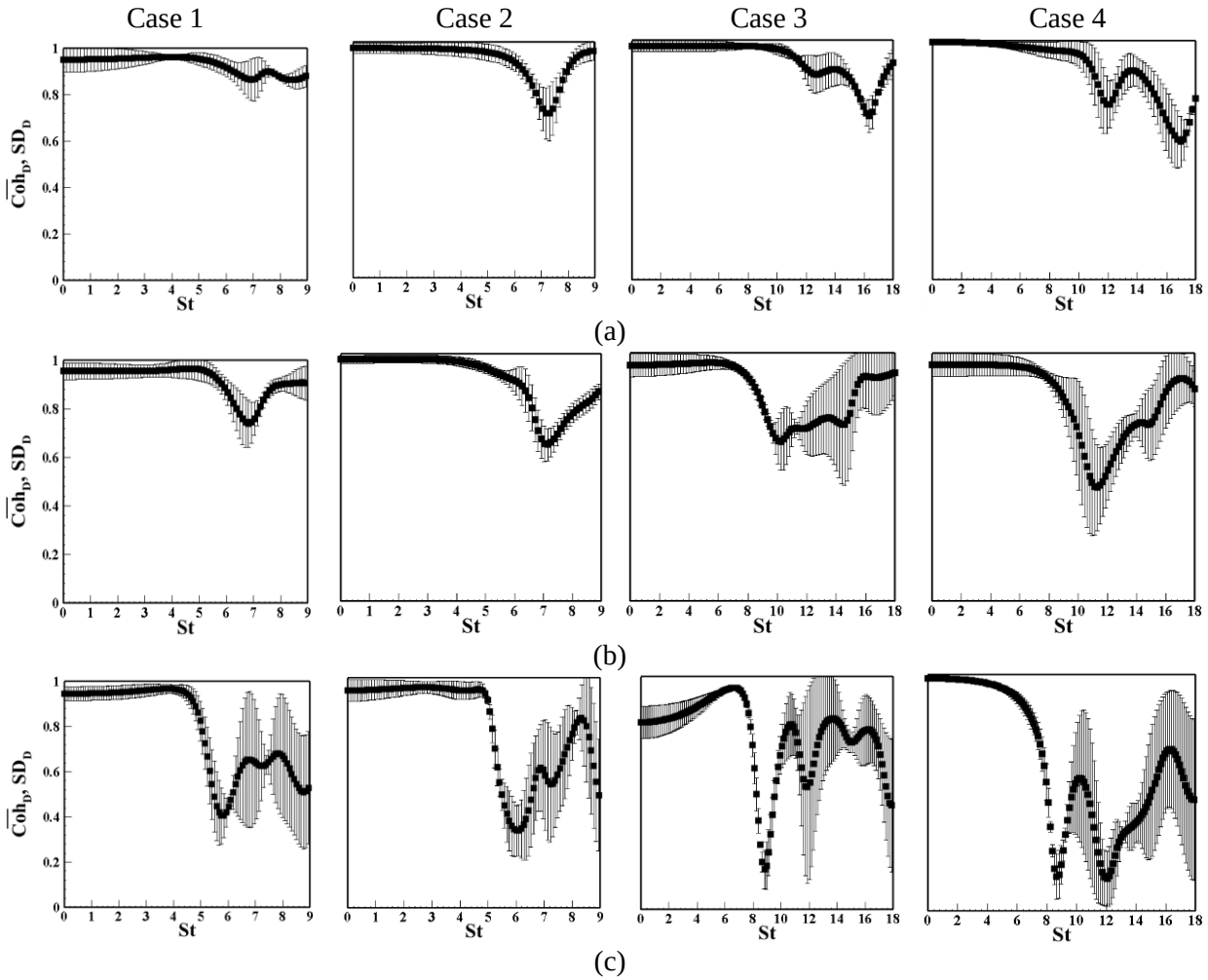

Fig. 10. Average coherence function, $\overline{Coh}_D$, (squares) and standard deviation, SD_D, (error bars) of the temperature signals obtained between TC1 and the other TCs for at (a) the inlet, (b) NZ1 outlet and (c) NZ2 outlet.

4.3. Detecting direct and indirect acoustic noise

This section aims to show the strength of direct and indirect noises and compare the two. The heat released from the heater expands the air passed over it. A pocket of expanded air can be a source of noise, called

direct noise, similar to any flame, which releases unsteady heat [2,47,48]. The hot pocket of air can further reach end of the pipe and enter the nozzle. The pocket accelerates through the nozzle and can be an extra source of noise, called indirect noise [4,5,6,49], as stated earlier in the Introduction. Although the indirect noise includes entropy, vortical and compositional division [33], only entropy noise is considered in the current study.

To measure the noises produced, three sensors were used, as Fig. 2b shows. A long pipe was also used to extend the distance between the heater and the nozzle. This elongates the convection length of the entropy wave and results in a time difference between the moments of two noises generation. The direct noise is generated just after heater turned on and propagates toward the sensors with the sound velocity, while the indirect noise exists only when the hot pocket of air reaches the nozzle. Therefore, longer convection distance of the entropy wave between the heater and the end nozzle aids to separately detect the direct and indirect noises. The flow velocity is further kept low, due to increasing the convection time of the entropy wave and making higher temporal lag between direct and indirect noise generation.

Fig. 11 depicts the acoustic variations detected at P1. This figure introduces the typical direct and indirect noise. It is noted that a very similar graph to Fig. 11 was reported in Ref. [33], in which the direct and indirect noise of a hot spot produced by an electrical heater were detected. The last part of the setup of Ref. [33] was an orifice plate and the pressure fluctuations were measured by two transducers located at the upstream and downstream of the orifice. Fig. 11 illustrates that a positive strong acoustic pulse is produced just after releasing the heating pulse ($t = 0.15s$), demonstrating a direct noise. After a while, the next peak in the pressure disturbance is detected at the time of arrival of the wave at the nozzle, providing an indirect noise with the negative amplitude. The temporal diversity between two noises generation can be calculated by the convection time of the entropy wave from the heater to the nozzle. The pressure increase may arise from the lower density of the base flow after passage of entropy wave [33]. This denotes that, as a sign of wave decay, some of the thermal energy of entropy wave is transmitted to the base flow and reduces the flow density. Fig. 12 presents the effect of increasing flow velocity (or Reynolds number) on the noise reflected into the test rig at P1. It should be noted that the acoustic tests were performed only using the nozzle with higher flow acceleration (NZ2) as it generated a stronger noise. Since the thermal power of the heater is constant, increasing the mass flow rate results in a decrement in the entropy wave amplitude. Nonetheless, both direct (positive pressure amplitude) and indirect noise (the negative pressure amplitude) increase by rising the flow velocity. This could be explained by noting the less annihilation of entropy wave as Reynolds number increases, which consequently leads to stronger entropy noise.

.

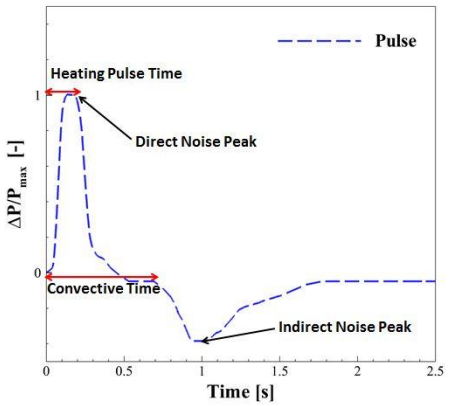

Fig. 11. Introducing the direct noise, indirect noise and convective time for the reflected wave at P1 location; the bulk flow velocity at the test rig inlet is 1.83m/s.

.

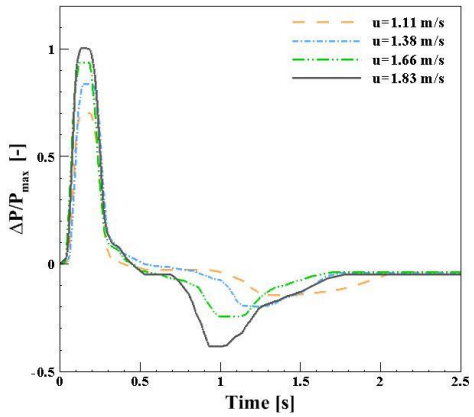

Fig. 12. Ensemble-averaged pressure signal detected by the differential sensors for various inlet bulk flow velocities of the test rig at location P1.

Fig. 13 shows the maximum noise amplitude for the four investigated cases. According to the uncertainty analysis presented in section 2.6, the error bars were added to Fig. 13, which is the only figure showing pressure discrete data. The decrement of the entropy noise from P2 to P1 is found insignificant. This is also valid for the direct noise, showing the acoustic wave deterioration while travelling through the gaseous medium of the test channel. The reflected noise, which one detected by P1 and P2 sensors in Fig. 2b, is higher than that of transmission, detected by P3 sensor in Fig. 2b, in qualitative agreement to the analytical work of Marble and Candel [5] and those of Fattahi and co-workers [19,20] for a subsonic flow. By considering the effects of Reynolds number and turbulence intensity on the entropy wave annihilation stated earlier [21,39], the acoustical differences among the cases can be explained. The entropy wave evolution, therefore, makes weaker resultant indirect noise, rendering a definitive conclusion upon the impact of entropy wave survival on the combustor acoustics.

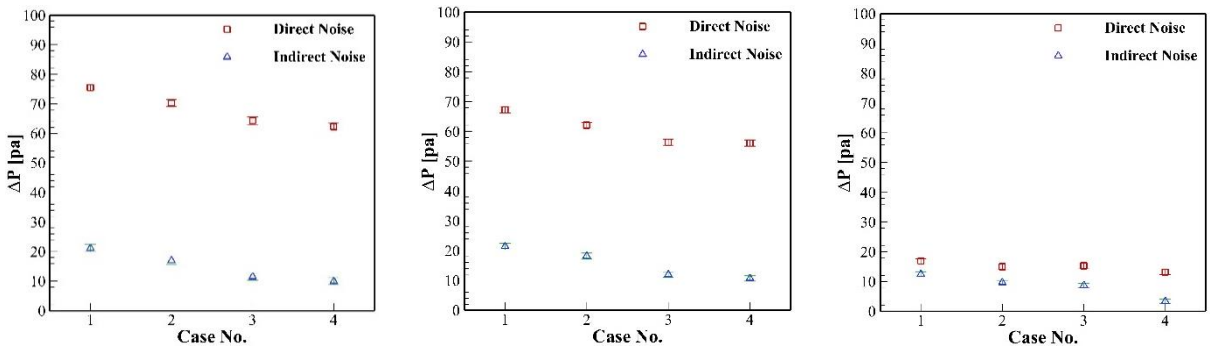

Fig. 13. Absolute values of the amplitude peak of direct and indirect noise for four cases at locations (a) P1, (b) P2 and (c) P3

The maximum amplitude of the indirect to direct noise ratio for three sensors of P1 to P3 and four cases of 1 to 4 is presented in Fig. 14. The indirect noise contribution is clearly decreased by either Reynolds number decrement or turbulence intensity increment, as the wave annihilation intensifies. The acoustical ratio calculated in locations P1 and P2 is about the same for all cases. The indirect noise contribution is more outstanding at the nozzle outlet than that at the inlet. It indicates that the transmission of the acoustic wave detected by sensor P3 is more significant than reflected acoustics measured by sensor P2. This is raised by the impedance of the nozzle boundary and shows the strong influences of the nozzle flow on the resultant acoustic waves. This figure shows where the weaker entropy wave evolution exists, the higher ratio of indirect to direct noise is found. In keeping with some previous results [25-27,31-33], Fig. 14 confirms that the indirect noise is a significant contributor to the overall noise generation.

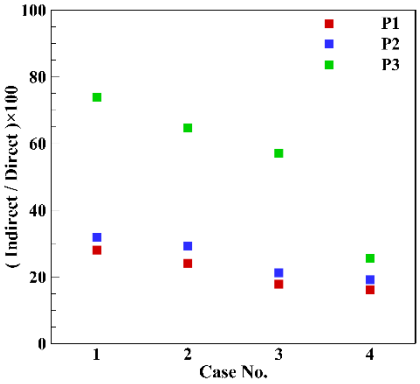

Fig. 14. The maximum amplitude of indirect to direct noise ratio at three locations and four cases studied.

Conclusions

Entropy noise is still the less-investigated source of combustion generated noise in gas turbines. To gain further insight into the physics of entropy noise, an experimental study was conducted on the convection of

entropy waves through subsonic nozzles. The decay of convecting temperature pulses, as entropy waves, was measured using the temperature-time trace recorded by the fast response thermocouples over a cross-section of the nozzle. For this purpose, the hydrodynamic parameters including Reynolds number and turbulence intensity were varied. The acoustic waves, produced by the entropy wave, were further measured to explore the effects of wave evolution on the conversion of entropy waves into sound. To the best of authors' knowledge, the present work is the first experimental analysis on the evolution of entropy waves in accelerating flows. The key findings of this study are as follows.

In keeping with the recent numerical results on the entropy wave evolution in duct flows [21,39], it was observed that increasing Reynolds number and decreasing turbulence intensity aid the wave survival. Also, the low frequency components of the entropy wave were less affected by the flow field. Calculating the spatial coherence function between the central and other thermocouples located at different radial and angular locations, the wave displayed a deviation from one-dimensionality. This indicates that the assumption of wave one-dimensionality, as commonly made in literature, can be readily violated in practice. It was further shown that the frequency threshold for the violation of this assumption is nearly constant for all cases. Increasing the flow acceleration made the wave more influenced by the hydrodynamics, rendering stronger spatio-temporal evolution of the entropy wave.

The measured pressure fluctuations presented an increasing trend versus velocity rising for both direct and indirect components of the noise. The indirect noises demonstrated the effects of hydrodynamics on the combustor acoustics, through making the entropy wave annihilated. It was shown that the indirect noise, caused by the passage of entropy wave through the nozzle, can generate pressure pulses that are quantitatively comparable to that of direct noise.

References

[1] Morgans, A.S. and Duran, I., 2016. Entropy noise: A review of theory, progress and challenges. International Journal of Spray and Combustion Dynamics, 8(4), pp.285-298.

[2] Candel, S., Durox, D., Schuller, T., Darabiha, N., Hakim, L. and Schmitt, T., 2013. Advances in combustion and propulsion applications. European Journal of Mechanics-B/Fluids, 40, pp.87-106.

[3] Candel, S., Durox, D., Ducruix, S., Birbaud, A.L., Noiray, N. and Schuller, T., 2009. Flame dynamics and combustion noise: progress and challenges. International Journal of Aeroacoustics, 8(1), pp.1-56.

[4] Williams, J.F. and Howe, M.S., 1975. The generation of sound by density inhomogeneities in low Mach number nozzle flows. Journal of Fluid Mechanics, 70(3), pp.605-622.

[5] Marble, F.E. and Candel, S.M., 1977. Acoustic disturbance from gas non-uniformities convected through a nozzle. Journal of Sound and Vibration, 55(2), pp.225-243.

[6] Cumpsty, N.A. and Marble, F.E., 1977. Core noise from gas turbine exhausts. Journal of Sound and Vibration, 54(2), pp.297-309.

[7] Cumpsty, N.A., 1979. Jet engine combustion noise: pressure, entropy and vorticity perturbations produced by unsteady combustion or heat addition. Journal of Sound and Vibration, 66(4), pp.527-544.
[8] Polifke, W., Paschereit, C.O. and Döbbeling, K., 2001. Constructive and destructive interference of acoustic and entropy waves in a premixed combustor with a choked exit. Int. J. Acoust. Vib, 6(3), pp.135-146.
[9] Goh, C.S. and Morgans, A.S., 2013. The influence of entropy waves on the thermoacoustic stability of a model combustor. Combustion Science and Technology, 185(2), pp.249-268.
[10] Huang, Y. and Yang, V., 2009. Dynamics and stability of lean-premixed swirl-stabilized combustion. Progress in energy and combustion science, 35(4), pp.293-364.
[11] Dowling, A.P. and Mahmoudi, Y., 2015. Combustion noise. Proceedings of the Combustion Institute, 35(1), pp.65-100.
[12] Ihme, M., 2017. Combustion and engine-core noise. Annual Review of Fluid Mechanics, 49, pp.277-310.
[13] Lefebvre, A.H., 1998. Gas turbine combustion. CRC press.
[14] Karimi, N., Brear, M.J. and Moase, W.H., 2008. Acoustic and disturbance energy analysis of a flow with heat communication. Journal of Fluid Mechanics, 597, pp.67-89.
[15] Karimi, N., Brear, M.J. and Moase, W.H., 2010. On the interaction of sound with steady heat communicating flows. Journal of Sound and Vibration, 329(22), pp.4705-4718.
[16] Goh, C.S. and Morgans, A.S., 2011. Phase prediction of the response of choked nozzles to entropy and acoustic disturbances. Journal of Sound and Vibration, 330(21), pp.5184-5198.
[17] Giauque, A., Huet, M. and Clero, F., 2012. Analytical analysis of indirect combustion noise in subcritical nozzles. Journal of Engineering for Gas Turbines and Power, 134(11), p.111202.
[18] Huet, M. and Giauque, A., 2013. A nonlinear model for indirect combustion noise through a compact nozzle. Journal of Fluid Mechanics, 733, pp.268-301.
[19] Fattahi, A., Hosseinalipour, S.M., Karimi, N., Saboohi, Z. and Ommi, F., 2019. On the response of a lean-premixed hydrogen combustor to acoustic and dissipative-dispersive entropy waves. Energy, 180, pp.272-291.
[20] Hosseinalipour, S.M., Fattahi, A. and Karimi, N., 2016. Investigation of the transmitted noise of a combustor exit nozzle caused by burned hydrogen-hydrocarbon gases. International Journal of Hydrogen Energy, 41(3), pp.2075-2086.
[21] Christodoulou, L., Karimi, N., Cammarano, A., Paul, M. and Navarro-Martinez, S., 2020. State prediction of an entropy wave advecting through a turbulent channel flow. Journal of Fluid Mechanics, 882.
[22] Zukoski, E.E. and Auerbach, J.M., 1976. Experiments concerning the response of supersonic nozzles to fluctuating inlet conditions. Journal of Engineering for Power, 98(1), pp.60-64.
[23] Hield, P.A., Brear, M.J. and Jin, S.H., 2009. Thermoacoustic limit cycles in a premixed laboratory combustor with open and choked exits. Combustion and Flame, 156(9), pp.1683-1697.
[24] Li, L., Zhao, D. and Yang, X., 2016. Effect of entropy waves on transient energy growth of flow disturbances in triggering thermoacoustic instability. International Journal of Heat and Mass Transfer, 99, pp.219-233.
[25] Bake, F., Richter, C., Mühlbauer, B., Kings, N., Röhle, I., Thiele, F. and Noll, B., 2009. The entropy wave generator (EWG): a reference case on entropy noise. Journal of Sound and Vibration, 326(3-5), pp.574-598.
[26] Bake, F., Michel, U. and Roehle, I., 2007. Investigation of entropy noise in aero-engine combustors. Journal of Engineering for Gas Turbines and Power, 129(2), pp.370-376.
[27] Bake, F., Kings, N. and Roehle, I., 2008. Fundamental mechanism of entropy noise in aero-engines: Experimental investigation. Journal of Engineering for Gas Turbines and Power, 130(1), p.011202.

[28] Hosseinalipour, S. M., A. Fattahi, H. Khalili, F. Tootoonchian, and N. Karimi. "Experimental investigation of entropy waves' evolution for understanding of indirect combustion noise in gas turbine combustors." Energy (2020): 116978.
[29] De Domenico, F., Shah, P., Lowe, S.M., Fan, L., Ewart, P., Williams, B.A. and Hochgreb, S., 2019. High frequency measurement of temperature and composition spots with LITGS. Journal of Engineering for Gas Turbines and Power, 141(3), p.031003.
[30] Sattelmayer, T., 2000, May. Influence of the combustor aerodynamics on combustion instabilities from equivalence ratio fluctuations. In ASME turbo expo 2000: power for land, sea, and air (pp. V002T02A003-V002T02A003). American Society of Mechanical Engineers.
[31] Rolland, E.O., De Domenico, F. and Hochgreb, S., 2017. Theory and application of reverberated direct and indirect noise. Journal of Fluid Mechanics, 819, pp.435-464.
[32] Rolland, E.O., De Domenico, F. and Hochgreb, S., 2018. Direct and indirect noise generated by entropic and compositional inhomogeneities. Journal of Engineering for Gas Turbines and Power, 140(8), p.082604.
[33] De Domenico, F., Rolland, E.O. and Hochgreb, S., 2017. Detection of direct and indirect noise generated by synthetic hot spots in a duct. Journal of Sound and Vibration, 394, pp.220-236.
[34] De Domenico, F., Rolland, E.O. and Hochgreb, S., 2019. A generalised model for acoustic and entropic transfer function of nozzles with losses. Journal of Sound and Vibration, 440, pp.212-230.
[35] Carolan, D., 2009. Measurement of the Transfer Function of a Combustor Exit Nozzle (Doctoral dissertation, University of Melbourne, Department of Mechanical Engineering).
[36] Morgans, A.S., Goh, C.S. and Dahan, J.A., 2013. The dissipation and shear dispersion of entropy waves in combustor thermoacoustics. Journal of Fluid Mechanics, 733.
[37] Eckstein, J., Freitag, E., Hirsch, C. and Sattelmayer, T., 2006. Experimental study on the role of entropy waves in low-frequency oscillations in a RQL combustor. Journal of Engineering for Gas Turbines and Power, 128(2), pp.264-270.
[38] Eckstein, J. and Sattelmayer, T., 2006. Low-order modeling of low-frequency combustion instabilities in aeroengines. Journal of propulsion and power, 22(2), pp.425-432.
[39] Fattahi, A., Hosseinalipour, S.M. and Karimi, N., 2017. On the dissipation and dispersion of entropy waves in heat transferring channel flows. Physics of Fluids, 29(8), p.087104.
[40] Weilenmann, M., Doll, U., Bombach, R., Blondé, A., Ebi, D., Xiong, Y. and Noiray, N., 2020. Linear and nonlinear entropy-wave response of technically-premixed jet-flames-array and swirled flame to acoustic forcing. Proceedings of the Combustion Institute.
[41] Weilenmann, M., Xiong, Y. and Noiray, N., 2020. On the dispersion of entropy waves in turbulent flows. Journal of Fluid Mechanics, 903.
[42] Wang, G., Liu, X., Wang, S., Li, L. and Qi, F., 2019. Experimental investigation of entropy waves generated from acoustically excited premixed swirling flame. Combustion and Flame, 204, pp.85-102.
[43] Webster, J.G. ed., 1999. The Measurement, Instrumentation, and Sensors: Handbook. Springer Science & Business Media.
[44] Figliola, R.S. and Beasley, D.E., 2020. Theory and design for mechanical measurements. John Wiley & Sons.
[45] D. C. Montgomery, G. C. Runger, "Applied statistics and probability for engineers," John Wiley & Sons, (2010).
[46] Goh, C.S. and Morgans, A.S., 2013. The influence of entropy waves on the thermoacoustic stability of a model combustor. Combustion Science and Technology, 185(2), pp.249-268.
[47] Mousavi, S.M., Kamali, R., Sotoudeh, F., Pourabidi, R., Karimi, N. and Jeung, I.S., 2019. A comprehensive investigation of acoustic power level in a moderate or intense low oxygen dilution in a jet-in-hot-coflow under various working conditions. Aerospace Science and Technology, 93, p.105339.

[48] Kumar, P.E. and Mishra, D.P., 2015. Combustion noise characteristics of an experimental 2D trapped vortex combustor. Aerospace Science and Technology, 43, pp.388-394.
[49] Fattahi, A., Karimi, N. and Hajialigol, N., 2020. Dynamics of entropy wave generation in a simplified model of gas turbine combustor: a theoretical investigation. Physics of Fluids. doi: 10.1063/5.0021729.